4

Salient pole permanent magnet axial-gap self-bearing motor

Quang-Dich Nguyen and Satoshi Ueno
Ritsumeikan University
Japan

1. Introduction

Recently, active magnetic-bearing motors have been designed to overcome the limitations of the conventional mechanical-bearing motors. Magnetic-bearing motors can work in all environments without lubrication and do not cause contamination; further, they can run at very high speeds. Therefore, they are very valuable machines with a number of novel features, and with a vast range of diverse applications (Dussaux, 1990).

The conventional magnetic-bearing motor usually has a rotary motor installed between two radial magnetic bearings, or a mechanical combination of a rotary motor and a radial magnetic bearing (The mechanically combined magnetic bearing motor usually has n-pole motor windings and n±2-pole suspension windings), as shown in Figs. 1 and 2 (Okada et al., 1996), (Oshima et al., 1996 a,b), (Zhaohui & Stephens, 2005), (Chiba et al., 2005). The radial magnetic bearings create radial levitation forces for rotor, while an axial magnetic bearing produces a thrust force to keep the rotor in the correct axial position relative to the stator. However, these magnetic-bearing motors are large, heavy, and complex in control and structure, which cause problems in applications that have limit space. Thus, a simpler and smaller construction and a less complex control system are desirable.

An axial magnetic bearing is composed of a rotary disc fixed on a rotary shaft and electromagnets arranged on both sides of the disc at a proper minute distance. This structure is similar to that of an axial-flux AC motor (Aydin et al., 2006), (Marignetti et al., 2008). Based on this, Satoshi Ueno has introduced an electrically combined motor-bearing which is shown in Fig. 3, in which the stator has only three-phase windings; however it can simultaneously provide non-contact levitation and rotation (Ueno & Okada, 1999), (Ueno & Okada, 2000). This motor is then called an axial-gap self-bearing motor (AGBM) to imply that the motor has self levitation function. Obviously, it is simpler in structure and control since hardware components can be reduced.

The AGBM can be realized as an induction motor (IM) (Ueno & Okada, 1999), or a permanent magnet (PM) motor (Ueno & Okada, 2000), (Okada et al., 2005), (Horz et al., 2006), (Nguyen & Ueno, 2009 a,b). The PM motor is given special attention, because of its high power factor, high efficiency, and simplicity in production.

In this chapter, the mathematical model of the salient 2-pole AGBM with double stators is introduced and analyzed (sandwich type). A closed loop vector control method for the axial position and the speed is developed in the way of eliminating the influence of the reluctance

torque. The vector control method for the AGBM drive is based on the reference frame theory, where the direct axis current i_d is used for controlling the axial force and the quadrate axis current i_q is used for controlling the rotating torque. The proposed control method is initially utilized for the salient AGBM ($L_{sd} < L_{sq}$), however it can be used for non-salient AGBM ($L_{sd} = L_{sq}$), too.

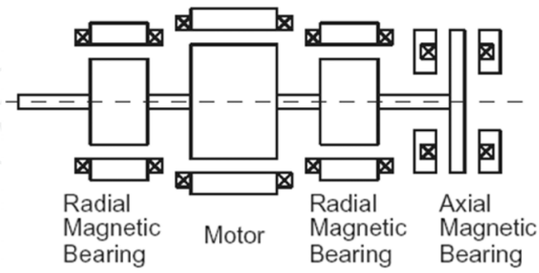

Fig. 1. Structure of conventional magnetic-bearing motor

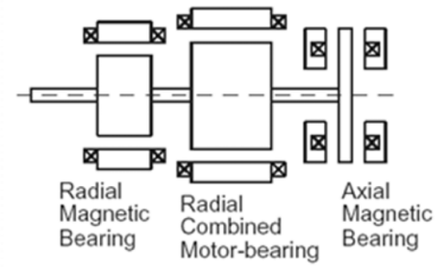

Fig. 2. Structure of radial-combined magnetic-bearing motor

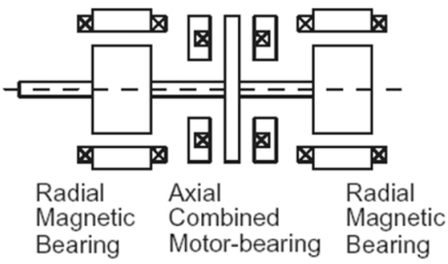

Fig. 3. Structure of axial-gap self-bearing motor

2. Mathematical Model

Per-phase equivalent circuits have been widely used in steady-state analysis of the AC machines. However, they are not appropriate to predict the dynamic performance of the motor. For vector control, a dynamic model of the motor is necessary. The analysis of three-phase motor is based on the reference frame theory. Using this technique, the dynamic equations of the AC motor are simplified and become similar to those of the DC motor.

The structure of an axial gap self-bearing motor is illustrated in Fig. 4. It consists of a disc rotor and two stators, which is arranged in sandwich type. The radial motions x, y, θ_x, and θ_y of the rotor are constrained by two radial magnetic bearings such as the repulsive bearing

shown. Only rotational motion and translation along the z axis are considered. The motor has two degrees of freedom (2 DOFs).

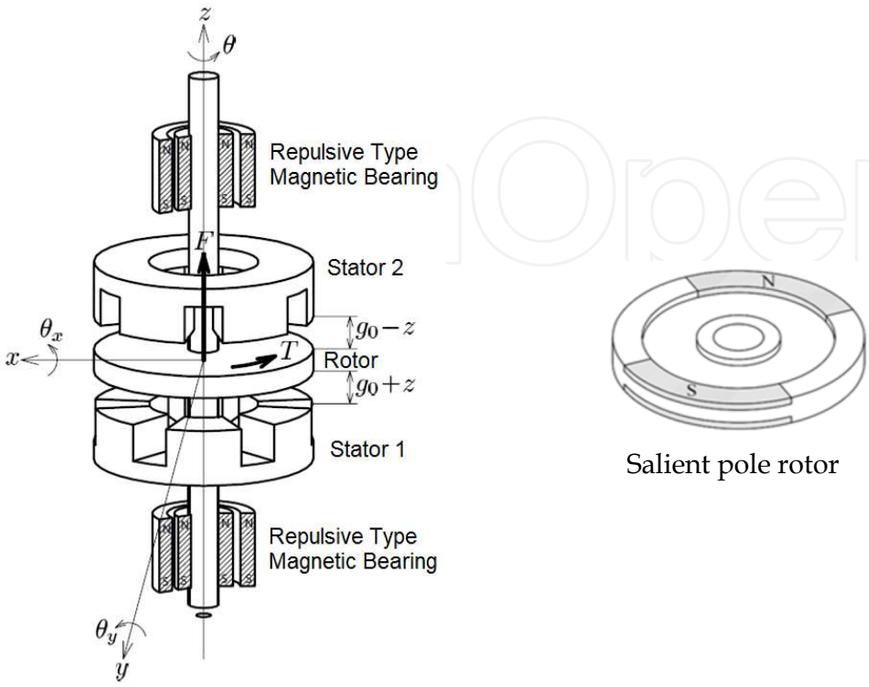

Fig. 4. Detail structure and coordinates of the AGBM

The rotor is a flat disc with PMs inserted on both faces of the disc to create a salient-pole rotor. Two stators, one in each rotor side, have three-phase windings that generate rotating magnetic fluxes in the air gap. These produce motoring torques T_1 and T_2 on the rotor and generate attractive forces F_1 and F_2 between the rotor and the stators. The total motoring torque T is the sum of these torques, and the axial force F is the difference of the two attractive forces.

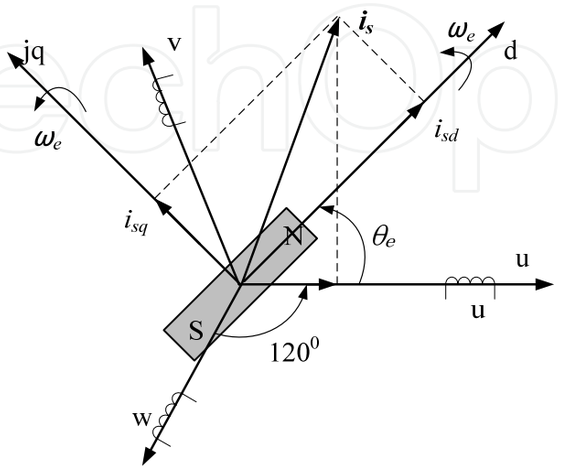

Fig. 5. Define of coordinates

To obtain a mathematical model of the AGBM, the axial force F_s and motoring torque T_s are first calculated for one stator. Similar to the non-salient AGBM, the mathematical model of the salient AGBM is presented in a rotor-field-oriented reference frame or so-called d, q coordinates, as indicated in Fig. 5. The d axis is aligned with the center lines of the permanent magnets and the q axis between the magnets. The axes u, v, and w indicate the direction of the flux produced by the corresponding phase windings. The phase difference between the u axis and the d axis is the electrical angular position θ_e of the rotor flux vector.

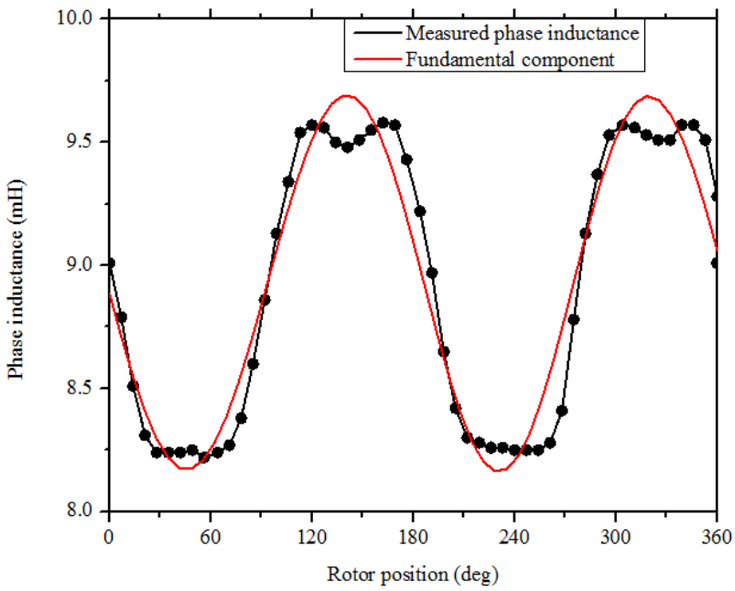

Fig. 6. Relation between phase inductance and rotor position

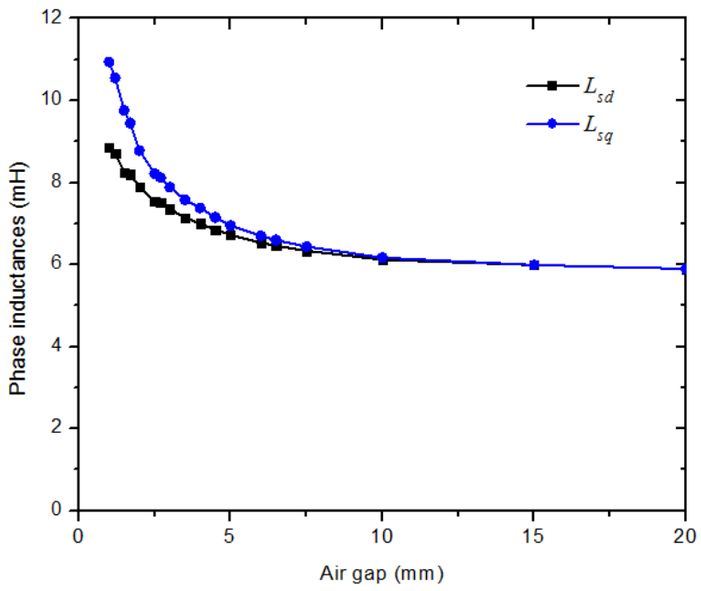

Fig. 7. Relation between phase inductance and air gap

Since the PM with unity permeability is used, the rotor is a salience; therefore the self-phase inductance of the stator is dependent on the rotor angular position, which means that the d-axis inductance is different from q-axis inductance. Furthermore, the self-phase inductance is a function of the air gap g between the rotor and the stator. The relation between self-phase inductance and rotor position as well as air gap is illustrated in Fig. 6 and 7. Obviously, the self-phase inductance is inversely proportional to the air gap, so the d- and q-axis phase inductance of the stator windings can be derived as (Fitzgerald, 1992)

$$\begin{cases} L_{sd} = \dfrac{3L'_{sd0}}{2g} + L_{sl} \\ L_{sq} = \dfrac{3L'_{sq0}}{2g} + L_{sl} \end{cases} \tag{1}$$

where, L'_{sd0}, L'_{sq0} are the d- and q-axis magnetizing inductances multiplied by the air gap length. They can be determined by calculating the motor parameters or measuring the phase inductance. L_{sl} is the leakage inductance. It can be estimated from the analysis of the measured phase inductance. By using the power invariant transformation method, the components of the stator voltage and the flux of the AGBM in the d,q coordinates can be expressed in the following equations:

$$\begin{cases} u_{sd} = R_s i_{sd} + L_{sd} \dfrac{di_{sd}}{dt} - \omega_e L_{sq} i_{sq} \\ u_{sq} = R_s i_{sq} + L_{sq} \dfrac{di_{sq}}{dt} + \omega_e L_{sd} i_{sd} + \omega_e \lambda_m \\ \lambda_{sd} = L_{sd} i_{sd} + \lambda_m \\ \lambda_{sq} = L_{sq} i_{sq} \end{cases} \tag{2}$$

where $\lambda_m = L_m i_f$ is the flux linkage caused by PM. For simplicity, the magnetic flux of the rotor is replaced by an equivalent winding with a DC current i_f and an inductance L_f. The rotor flux can be expressed only in d axis as follows:

$$\lambda_f = \lambda_{fd} = i_f L_f + L_m i_{sd} \tag{3}$$

with

$$L_f = \frac{3}{2} \frac{L'_{sd0}}{g} + L_{sl} \tag{4}$$

and mutual inductance

$$L_m = \frac{3L'_{sd0}}{2g} \tag{5}$$

From (2) to (5), the magnetic co-energy in the air gap for a stator is calculated as follows:

$$\begin{aligned} W &= \frac{1}{2}(\lambda_f i_f + \lambda_{sd} i_{sd} + \lambda_{sq} i_{sq}) \\ &= \frac{1}{2}\left\{L_{sd}\left(i_f^2 + i_{sd}^2\right) + L_{sq} i_{sq}^2 + 2L_m i_{sd} i_f\right\} \end{aligned} . \tag{6}$$

$$\Rightarrow W = \frac{1}{2}\left\{\left(\frac{3}{2}\frac{L'_{sd0}}{g} + L_{sl}\right)\left(i_f + i_{sd}\right)^2 + \left(\frac{3}{2}\frac{L'_{sq0}}{g} + L_{sl}\right) i_{sq}^2\right\} \tag{7}$$

Therefore, the attractive force of one stator is received by the derivative of the magnetic co-energy with respect to the axial displacement:

$$F_s = \frac{\partial W}{\partial z} = -\frac{3L'_{sd0}}{4g^2}\frac{dg}{dz}\left(i_{sd} + i_f\right)^2 - \frac{3L'_{sq0}}{4g^2}\frac{dg}{dz} i_{sq}^2 \tag{8}$$

and the motoring torque for one stator is calculated as follows:

$$\begin{aligned} T_s &= P(-\lambda_{sd} i_{sq} + \lambda_{sq} i_{sd}) \\ &= \frac{3PL'_{sd0}}{2g} i_f i_{sq} + \frac{3P(L'_{sd0} - L'_{sq0})}{2g} i_{sd} i_{sq} = T_{seff} + T_{srl} \end{aligned} \tag{9}$$

where

P is the number of pole pairs

$T_{seff} = \frac{3PL'_{sd0}}{2g} i_f i_{sq}$ is the effective torque caused by q-axis current

$T_{srl} = \frac{3P(L'_{sd0} - L'_{sq0})}{2g} i_{sd} i_{sq}$ is the reluctance torque caused by the different between d- and q-axis inductances.

From (9), the output torque of the AGBM is a combination of an excitation torque and a reluctance torque. That means, in every operation mode, the motor has to produce an additional torque to compensate the reluctance torque. In the non-salient pole rotor, this reluctance torque can be ignored to make control system simpler. However, in the salient-pole rotor when the reluctance torque can reach the relative high amplitude, the neglect of this torque component will reduce the quality of system, especially in operation mode with axial load ($i_d \neq 0$).

From (8) and (9) F_1 and T_1 are calculated by substituting $g = g_0 + z$, $i_{sd} = i_{d1}$, and $i_{sq} = i_{q1}$, and F_2 and T_2 are calculated by substituting $g = g_0 - z$, $i_{sd} = i_{d2}$, and $i_{sq} = i_{q2}$. Thus, the total axial force F and torque T are given by:

$$\begin{aligned} F &= F_2 + F_1 \\ &= \frac{3L'_{sd0}}{4(g_0 - z)^2}\left(i_{d2} + i_f\right)^2 + \frac{3L'_{sq0}}{4(g_0 - z)^2} i_{q2}^2 - \frac{3L'_{sd0}}{4(g_0 + z)^2}\left(i_{d1} + i_f\right)^2 - \frac{3L'_{sq0}}{4(g_0 + z)^2} i_{q1}^2 \end{aligned} \tag{10}$$

$$\begin{aligned} T &= T_1 + T_2 \\ &= \frac{3PL'_{sd0}}{2(g_0 + z)} i_f i_{q1} + \frac{3P(L'_{sd0} - L'_{sq0})}{2(g_0 + z)} i_{d1} i_{q1} + \frac{3PL'_{sd0}}{2(g_0 - z)} i_f i_{q2} + \frac{3P(L'_{sd0} - L'_{sq0})}{2(g_0 - z)} i_{d2} i_{q2} \end{aligned} \tag{11}$$

where g_0 is the axial gap at the equilibrium point and z is the displacement.

For linearization at the equilibrium point (z = 0), (10) and (11) are expanded into a Maclaurin series and the first-order term is taken, yielding:

$$\begin{aligned} F = {} & K_{Fd}\left\{\left(i_{d2} + i_f\right)^2 - \left(i_{d1} + i_f\right)^2\right\} + K_{Fq}\left(i_{q2}^2 - i_{q1}^2\right) + \\ & + 2K_{Fd}\left\{\left(i_{d2} + i_f\right)^2 + \left(i_{d1} + i_f\right)^2\right\} z / g_0 \; + 2K_{Fq}\left(i_{q2}^2 + i_{q1}^2\right) z / g_0 \end{aligned} \tag{12}$$

$$T = K_T\left(i_{q1} + i_{q2}\right) + K_T\left(i_{q2} - i_{q1}\right) z / g_0 + K_R\left(i_{d1} i_{q1} + i_{d2} i_{q2}\right) + K_R\left(i_{d2} i_{q2} - i_{d1} i_{q1}\right) z / g_0 \tag{13}$$

where

$K_{Fd} = \dfrac{3L'_{sd0}}{4g_0^2}$ and $K_{Fq} = \dfrac{3L'_{sq0}}{4g_0^2}$ are the force factors,

$K_T = -\dfrac{3PL'_{sd0} i_f}{2g_0}$ and $K_R = -\dfrac{3\left(L'_{sd0} - L'_{sq0}\right)}{2g_0}$ are the torque factors.

To increase the total moment twice the component moment created by one stator, the moment-generated currents for both stators must be same direction and value. To keep the rotor in right position between two stators, the forces acting on rotor from both sides must be same value but inverse, i.e. under the effect of the axial load, if the force-generated current of one side increases, then correspondingly, that current of other side has to decrease the same amount. The rotating torque can be controlled effectively by using the quadrate-axis current, and the axial force can be controlled by changing the direct-axis current. It is supposed that:

$$\begin{cases} i_{q1} = i_{q2} = i_q \\ i_{d1} = i_{d0} - i_d \\ i_{d2} = i_{d0} + i_d \end{cases} \tag{14}$$

where i_{d0} is an offset current, and the value can be zero or a small value around zero.

Inserting (14) into (12) and (13) yields:

$$T = 2K_T i_q + 2K_R i_{d0} i_q + 2K_R i_d i_q \frac{z}{g_0} = T_{eff} + T_{rl0} + T_{rlz} \tag{15}$$

$$\begin{aligned} F &= 4K_{Fd}(i_f + i_{d0})i_d + \\ &+ 4\left\{K_{Fd}(i_d^2 + i_{d0}^2 + i_f^2) + 2K_{Fd} i_f i_{d0} + K_{Fq} i_q^2\right\}\frac{z}{g_0} \end{aligned} \tag{16}$$

From (15), the total torque consists of three components.

1) The first component, $T_{eff} = 2K_T i_q$, is the efficient torque of the AGBM, this is main component of the output torque, which is caused by the interaction between PM flux and stator flux.
2) The second one, $T_{rl0} = 2K_R i_{d0} i_q$, is the reluctance torque caused by current i_{d0}. Therefore, assuming that $i_{d1} = -i_{d2} = -i_d$ *i.e.* $i_{d0} = 0$ then this reluctance torque is eliminated.
3) The last one, $T_{rlz} = 2K_R i_d i_q z / g_0$, is reluctance torque caused by current i_d under the effect of the displacement z. When the displacement is well controlled to be zero, or very small in comparison with air gap at the equilibrium point g_0, the influence of this component can be neglected.

As the result, the total torque becomes as follows:

$$T = 2K_T i_q \tag{17}$$

Obviously, the effect of the inductance difference to the total torque is vanished.
Using the control law (14), the total axial force is received from (16) when $i_{d0} = 0$ as

$$F = 4K_{Fd} i_f i_d + 4\left\{K_{Fd}(i_d^2 + i_f^2) + K_{Fq} i_q^2\right\} z / g_0 \tag{18}$$

When the displacement is zero or very small in comparison with air gap at the equilibrium point g_0, the total torque becomes

$$F = 4K_{Fd} i_f i_d \tag{19}$$

From (17) and (19), it is easy to see that the total torque is proportional with the quadrate axis current and the axial force is proportional with the direct axis current. Although the axial force depends lightly on the quadrature axis current, its main component is proportional to the direct axis current, so a decoupled d- and q-axis current control system can be implemented to control the axial force and motoring torque independently.

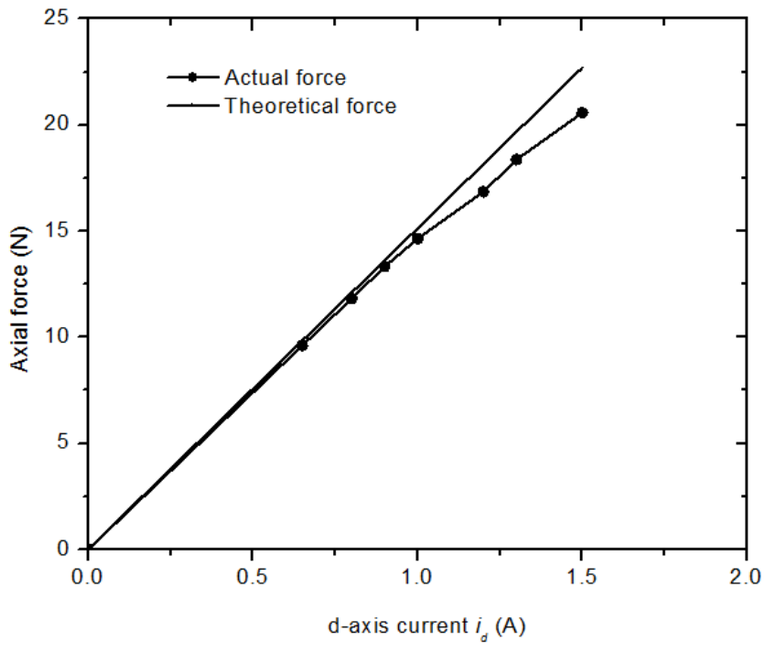

Fig. 8. Relation between axial force and d-axis current

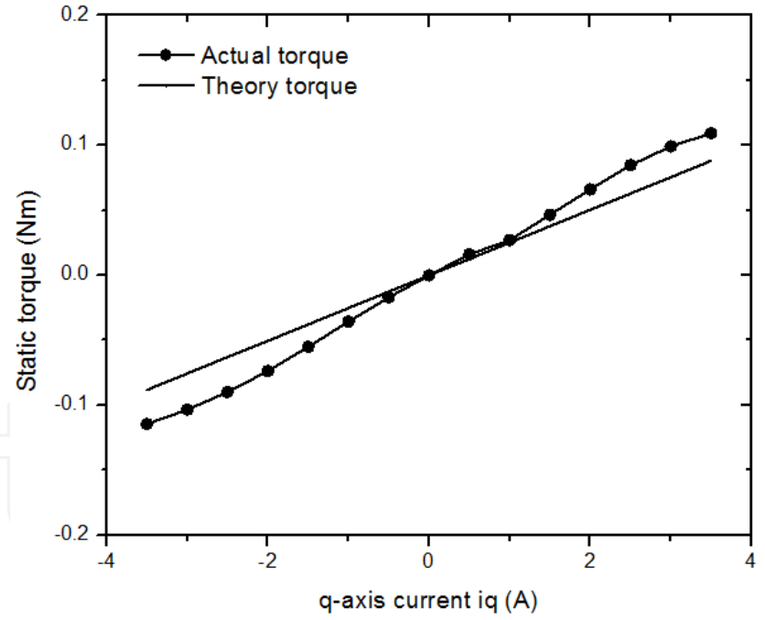

Fig. 9. Relation between rotational torque and q-axis current

From (2), (3), (17) and (19), the mathematical model of the AGBM is completely constructed with voltage, force, and torque equations. It can be seen that these are simple linear equations, so the control system can be easily implemented with conventional controllers.

3. Vector Control Structure

3.1 Generality

Vector control of the AGBM is based on decomposition of the instantaneous stator current into two components: axial force-producing current i_d (also flux current) and torque-producing current i_q. By this way the control structure of the AGBM becomes similar to that of the DC motor.

As stated above, the motoring torque of the AGBM can be controlled by the q-axis current (i_q), while the axial force can be controlled by the d-axis current (i_d). Fig. 10 shows the control scheme proposed for the AGBM drive with decoupled current controller.

The axial displacement from the equilibrium point along the z-axis, z, can be detected by the gap sensor. The detected axial position is compared with the axial position command z_{ref} and the difference is input to the axial position controller R_z. The position command z_{ref} is always set to zero to ensure the rotor is at the midpoint between the two stators. The output of the axial position controller is used to calculate the d-axis reference current i_{dref}. The d-axis reference currents for the two stator windings i_{d1ref} and i_{d2ref} can be generated by using the offset current i_{d0} and respectively subtracting or adding i_{dref}. The value of the offset current can be zero or a small value around zero.

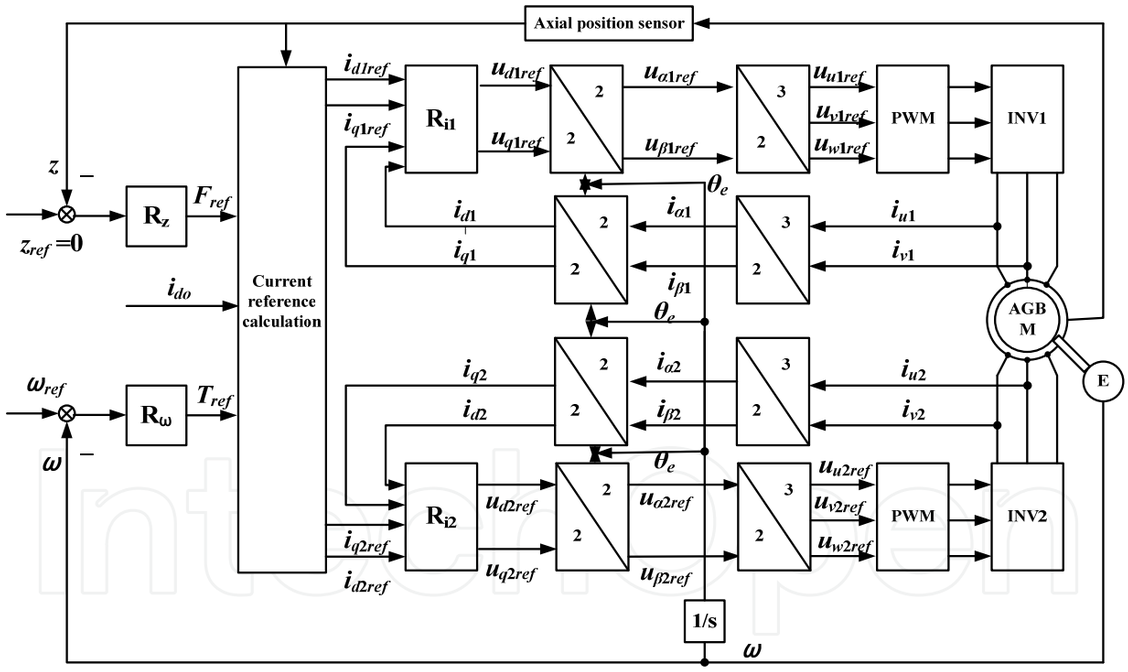

Fig. 10. Control structure for the AGBM.

The rotor speed detected from the encoder is compared with the reference speed and the difference is input to the speed controller R_ω. The output of the speed controller is used to calculate the q-axis reference current i_{qref}. The q-axis reference currents for the two stator windings i_{q1ref} and i_{q2ref} are then set the same as the calculated current i_{qref}.

The motor currents in the two-phase stator reference frame α,β are calculated by measuring two actual phase currents. Consequently, the d,q components are obtained using the rotor

position from the encoder. The quadrature components are controlled by the reference value that is given by the speed controller, while the direct components are controlled by the reference value that is given by the axial position controller. The outputs of the current controllers, representing the voltage references, are subsequently directed to the motor using the pulse width modulation (PWM) technique, once an inverse transformation from the rotating frame to the three-phase stator reference frame has been performed. All the controllers are PI controller except that the axial position controller is PID.

3.2 Current Control

Most of the modern AC motor drives have a control structure comprising an internal current control loop. Consequently, the performance of the drive system largely depends on the quality of applied current control strategy.

The main task of the current control loop is to force the current in a three-phase motor to follow the reference signals. By comparing the reference currents and measured currents, the current control loop generates the switching states for the inverter which decrease the current errors. Hence, in general the current control loop implements two tasks: *error compensation* (decrease current error) and *modulation* (determine switching states).

The design of the current controllers in the simplest cases of so-called parametric synthesis of linear controllers is limited to the selection of a controller type such as P, PI or PID and the definition of optimal setting of its parameters according to the criterion adopted. This design is normally done with complete knowledge of the controlled object and is described in many literatures (Kazmierkowski & Melasani, 1998), (Gerd, 2004).

From equation (2), the stator voltage equations are rewritten in a slightly different form as follows:

$$\begin{cases} u_{sd} = \left(R_s + sL_{sd}\right) i_{sd} - \Delta u_{sd} \\ u_{sq} = \left(R_s + sL_{sq}\right) i_{sq} + \Delta u_{sq} \end{cases} \tag{20}$$

with s is laplace operator and

$$\begin{cases} \Delta u_{sd} = \omega_e L_{sq} i_{sq} \\ \Delta u_{sq} = \omega_e L_{sd} i_{sd} + \omega_e \lambda_m \end{cases} \tag{21}$$

Equations (20) and (21) describe a coupled system. In actual, the current control loop is much faster than a change of the rotor speed and rotor flux, therefore decoupling of the two current controllers can be achieved by adding voltages Δu_{sd} and Δu_{sq} at the output of the current controllers compensating the cross coupling in the motor.

The structure of the current control loop is shown in Fig. 11.

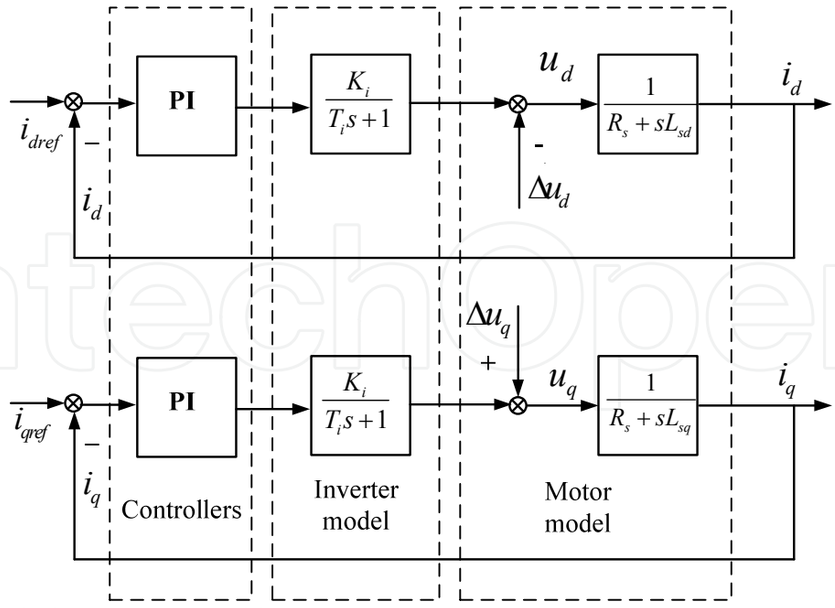

Fig. 11. Decoupled current control loop

Due to the difference between the d- and q-axis inductance, the current control design for i_d and i_q is performed separately.

The decoupled current control loop of the d-axis current contains a dominant stator time constant $T_s = L_{sd}/R_s$ and an inverter time constant T_i. The latter is the time required for the conversion of the reference voltage to the inverter output voltage, mainly depending on the constant sample time τ_s and PWM frequency $f_{PWM} = 1/T_{PWM}$:

$$T_i = \tau_s + T_{PWM} \tag{22}$$

Due to the similarity of the control structure, the design of current controller is only made for one current control loop, the other current control loops are obtained similarly.

Considering that the PI controller is utilized for current control, the open-loop transfer function of both d-axis and q-axis is:

$$G_{0i}(s) = K_{pd}\frac{T_{id}s+1}{T_{id}s}\frac{K_i}{T_i s+1}\frac{1}{T_{sd}s+1}\frac{1}{R_s} \tag{23}$$

According to optimal modulus criterion, the time constant T_{id} of the PI controller within such system is optimally chosen to neutralize the largest time constant in the loop:

$$T_{id} = T_{sd} \tag{24}$$

The optimum value of the controller gain is chosen as follows:

$$K_{pd} = \frac{R_s T_{id}}{2K_i T_i} \tag{25}$$

Consequently, the closed-loop transfer function of the d-axis current control loop becomes:

$$G_{si}(s) = \frac{i_d}{i_{dref}} = \frac{G_{0i}}{G_{0i}+1} = \frac{1}{2T_i^2 s^2 + 2T_i s + 1} \tag{26}$$

For the overlaid axial displacement control loop, the closed-loop transfer function is often simplified to a first order system with an equivalent time constant $T_{eq} = 2\sqrt{2}T_i$:

$$G_{si}(s) = \frac{i_d}{i_{dref}} = \approx \frac{1}{T_{eq}s + 1} \tag{27}$$

By the same way, the parameters of the q-axis current controller are as follows

$$\begin{cases} T_{iq} = T_{sq} \\ K_{pq} = \dfrac{R_s T_{iq}}{2K_i T_i} \end{cases} \tag{28}$$

and the closed-loop transfer function of the q-axis current control loop used for overlaid speed control loop becomes:

$$G_{si}(s) = \frac{i_q}{i_{qref}} = \approx \frac{1}{T_{eq}s + 1} \tag{29}$$

3.3 Axial Displacement Control

For simplicity, it is assumed that the radial motion of the rotor is restricted by two ideal radial bearings. Therefore, the axial motion is independent of the radial motion and can be expressed as follows:

$$F - F_L = m\ddot{z} \tag{30}$$

where m is the mass of the moving parts and F is the axial force. Then substituting (18) into (30) yields

$$m\ddot{z} + F_L = 4K_{Fd} i_f i_d + 4\left\{K_{Fd}\left(i_f^2 + i_d^2\right) + K_{Fq} i_q^2\right\}\frac{z}{g_0}. \tag{31}$$

This can be summarized as

$$m\ddot{z} + F_L + K_z z = K_m i_d \tag{32}$$

where

$K_z = -4\left\{K_{Fd}\left(i_f^2 + i_d^2\right) + K_{Fq} i_q^2\right\} / g_0$ is the stiffness of the motor, and

$K_m = 4K_{Fd} i_f$ is the force gain.

It is easy to see that K_z is negative, which means that this system is unstable. To stabilize the system, a controller with the derivative component must be used. The axial displacement control loop is shown in Fig. 12.
The axial displacement control loop contains the closed-loop transfer function of the inner d-axis current control loop and axial motion function. Since the axial load is usually unknown, it is handled in a first step as an external system disturbance.
Assuming that the proportional derivative controller (PD) is used, the output of the axial position controller will represent the direct axis reference current, i.e.,

$$i_d = -K_P z - K_D \dot{z} \tag{33}$$

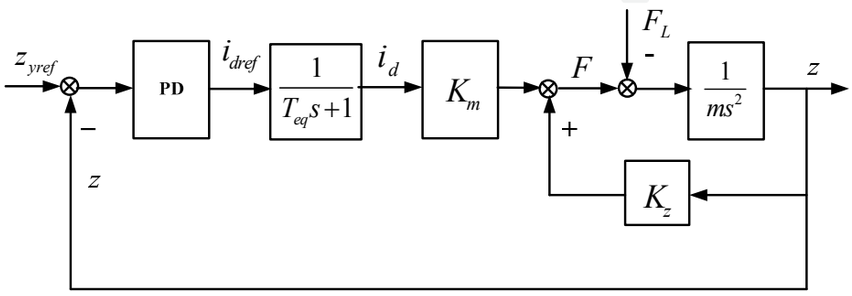

Fig. 12. Axial displacement control loop

where K_p is the proportional constant and K_d is the derivative constant of the axial position controller. Substituting (33) into (32) gives

$$m\ddot{z} + K_m K_D \dot{z} + \left(K_z + K_m K_P\right) z = 0 . \tag{34}$$

The system becomes stable only when all the constant coefficients of the polynomial function have the same sign. Therefore, if $K_d > 0$, the system will be stable if the proportional constant satisfies the condition

$$\begin{cases} K_P > -\dfrac{K_z}{K_m} = \dfrac{K_{Fd}\left(i_f^2 + i_d^2\right) + K_{Fq} i_q^2}{K_{Fd} i_f g_0} \\ K_D > 0 \end{cases} . \tag{35}$$

Steady-state error occurs when only the PD controller is used, and to remove this, a PID controller should be used. The transfer function of the PID controller is expressed as follows:

$$G_{cz}(s) = K_P + \frac{K_I}{s} + K_D s \tag{36}$$

By the same way as stated above, the system will be stable when the controller parameters satisfy:

$$\begin{cases} K_P > \dfrac{K_{Fd}\left(i_f^2 + i_d^2\right) + K_{Fq} i_q^2}{K_{Fd} i_f g_0} \\ K_I < \dfrac{K_D\left(K_m K_P + K_z\right)}{m} \\ K_I > 0 \\ K_D > 0 \end{cases} \tag{37}$$

In practice, the output of an ideal derivative element unfortunately includes considerable noise. High frequency noise at the input terminals results in significant amplification at the output terminals, therefore the ideal derivative element should be avoided in practical implementation. The practical controller function is expressed as follows:

$$G_{cz}(s) = K_P + \frac{K_I}{s} + \frac{K_D s}{T_f s + 1} \tag{38}$$

The denominator determines the high frequency limit with the cut-off frequency as $1/T_f$ and the numerator acts as a derivative function in the angular frequency range higher than $1/K_D$; therefore, the practical PID controller executes as a derivative function in a frequency range from $1/K_D$ to $1/T_f$. The low frequency gain is 0 dB and the high frequency gain is limited to K_D / T_f, hence T_f can be chosen from the actual signal condition.

In discrete time, equation (31) can be expressed as:

$$G_{cz}(s) = K_P + \frac{K_I \tau_s \left(z+1\right)}{2\left(z-1\right)} + \frac{2K_D\left(z-1\right)}{\left(2T_f + \tau_s\right)z - \left(2T_f - \tau_s\right)} \tag{39}$$

when the bilinear transform method is utilized.

3.4 Speed Control

For all motor types, the difference of electromagnetic torque T and load torque T_L causes acceleration of the rotor according to the mechanical property of the motor drives. The rotational motion equation can be written as:

$$T - T_L = J\frac{d\omega}{dt}, \tag{40}$$

or in fixed transfer function:

$$\frac{\omega}{T - T_L} = \frac{1}{Js} \tag{41}$$

Torque can be controlled by the q-axis current as shown in equation (16); therefore, the speed control loop is shown in Fig. 13.

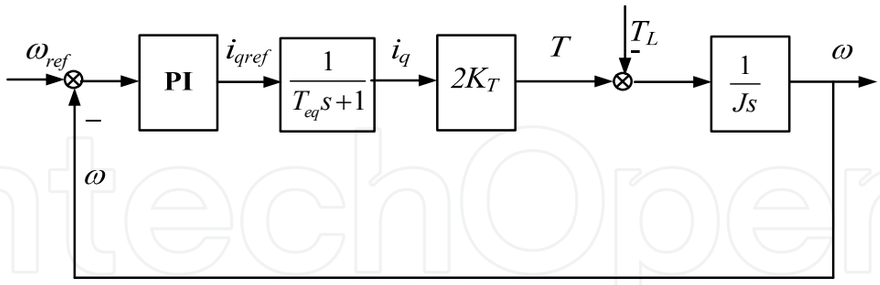

Fig. 13. Speed control loop

Like the axial displacement control loop, the speed control loop also contains the inner q-axis current control loop and rotational motion function. Since the rotational load is unknown, it is handled in a first step as an external system disturbance. The influence of the speed measurement is usually combined with the equivalent time constant of the current control.
Consequently, the resulting speed loop to be controlled is:

$$\frac{\omega}{i_{qref}} = \frac{2K_T}{T_{eq}s+1}\frac{1}{Js} \tag{42}$$

The simplest speed controller is a proportional controller (P), converting the speed error in the q-axis current command i_{qref}. Assuming no load (T_L=0), a positive speed error creates positive electromagnetic torque accelerating the drive until the error vanishes, and a negative speed error gives negative electromagnetic torque decelerating the drive until the error vanishes (braking mode). Thus, the steady-state error is zero in the no-load case. When the P-controller is used, the closed-loop transfer function is:

$$\frac{\omega}{\omega_{ref}} = \frac{1}{1+\frac{J}{2K_TK_p}s+\frac{JT_{eq}}{2K_TK_p}s^2} = \frac{1}{1+2\xi\left(\frac{s}{\omega_n}\right)+\left(\frac{s}{\omega_n}\right)^2} \tag{43}$$

with:

$$\omega_n = \sqrt{\frac{2K_TK_p}{JT_{eq}}} \text{ is the natural angular frequency, and} \tag{44}$$

$$\xi = \sqrt{\frac{J}{8K_TK_pT_{eq}}} \text{ is the damping constant.} \tag{45}$$

From these equations, it can be seen that the speed response to the external torque is determined by the natural angular frequency. Faster response is obtained at higher ω_n, while strong damper is achieved at higher ζ. For arriving at a compromise, the optimum gain of the current control is chosen as:

$$K_P = \frac{J}{4K_T T_{eq}} \text{ when the damping constant } \xi = 1/\sqrt{2}\,. \tag{46}$$

However, a simple P controller yields a steady-state error in the presence of rotational load torque, this error can be estimated as:

$$e_\omega = \left(\omega_{ref} - \omega\right)\Big|_{t\to\infty} = \frac{T_L}{K_p} \tag{47}$$

The most common approach to overcome this problem is applying an integral-acting part within the speed controller. The speed controller function is expressed as:

$$G_{c\omega}(s) = K_p\left(\frac{1+T_{i\omega}s}{T_{i\omega}s}\right) \tag{48}$$

Then the open-loop transfer function of speed loop is:

$$G_{0\omega}(s) = K_p \frac{1+T_{i\omega}s}{T_{i\omega}s}\frac{2K_T}{T_{eq}s+1}\frac{1}{Js} \tag{49}$$

Similar to the current control, the calculation of the controller parameters $K_{1\omega}$ and $T_{1\omega}$ depend on the system to be controlled. For optimum speed response, parameter calculation is done according to symmetrical optimization criterion. The time constant $T_{1\omega}$ of the speed controller is chosen bigger than the largest time constant in the loop, and the gain is chosen so that the cut-off frequency is at maximum phase. The results can be expressed as:

$$\begin{cases} T_{i\omega} = 20T_{eq} \\ K_p = \dfrac{J}{2K_T\sqrt{T_{i\omega}T_{eq}}} \end{cases} \tag{50}$$

4. Experimental Results

4.1 Hardware

To demonstrate the proposed control method for a PM-type AGBM, an experimental setup was constructed; it is shown schematically in Fig. 14. The rotor disc, shown in Fig. 15, has a diameter of 50mm. Four neodymium magnets with a thickness of 1mm for each side are mounted to the disc's surfaces to create two pole pairs. In this paper, only rotational motion of the rotor and translation of the stator along the z axis are considered, hence for a more simple experiment, the rotor is supported by two radial ball bearings that restrict the radial motion.
The stator, shown in Fig. 16, has a core diameter 50 mm and six concentrated wound poles, each with 200 coil turns. The stators can slide on the linear guide to ensure a desired air gap between the rotor and the two stators. A DC generator (Sanyo T402) is installed to give the load torque. A rotary encoder (Copal RE30D) measures the rotor angle and an eddy-current-type displacement sensor (Shinkawa VC-202N) measures the axial position.

The control hardware of the AGBM drive is based on a dSPACE DS1104 board dedicated to the control of electrical drives. It includes PWM units, general purpose input/output units (8 ADC and 8 DAC), and an encoder interface. The DS1104 reads the displacement signal from the displacement sensor via an A/D converter, and the rotor angle position and speed from the encoder via an encoder interface. Two motor phase currents are sensed, rescaled, and converted to digital values via the A/D converters. The DS1104 then calculates reference currents using the rotation control and axial position control algorithms and sends its commands to the three-phase inverter boards. The AGBM is supplied by two three-phase PWM inverters with a switching frequency of 20 kHz.

Stator phase resistance R_s	2.6 Ω
Effective inductance per unit gap in d axis L'_{sd0}	8.2e-6 Hm
Effective inductance per unit gap in q axis L'_{sq0}	9.6e-6 Hm
Leakage inductance L_{sl}	6e-3 H
Inertial moment of rotor J	0.00086 kgm²
Number of pole pairs P	1
Permanent magnet flux λ_m	0.0126 Wb

Table 1. Parameters of salient pole AGBM

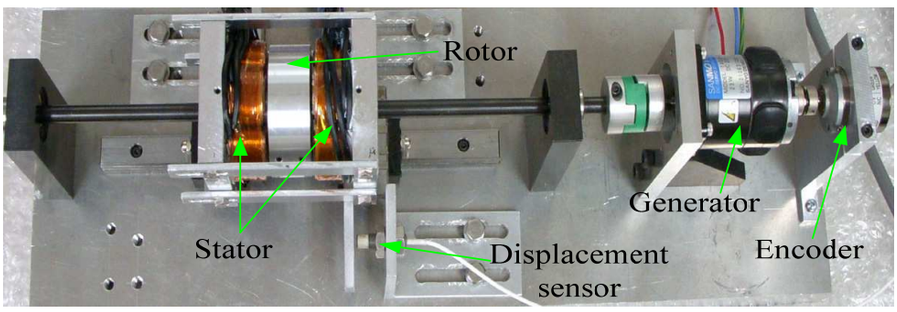

Fig. 14. Picture of the experimental setup

Fig. 15. Picture of the rotor of the AGBM

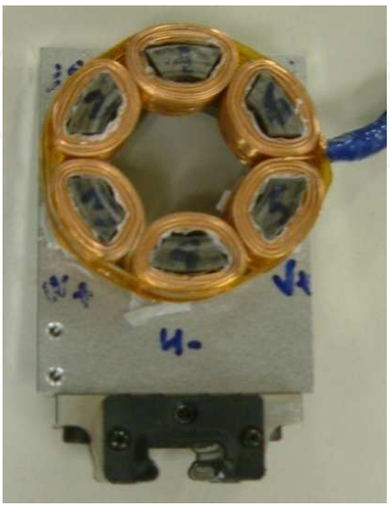

Fig. 16. Picture of the stator of the AGBM

4.2 Response of Speed and Axial Displacement

Fig. 17 shows the axial displacement at 0 rpm. The original displacement is set to 0.32 mm, and at the time of 0.45 s, the axial position controller starts to work. In transient state, the maximum error is 0.05 mm, much smaller than the air gap at the equilibrium point (g_0 = 1.7mm) and the settling time is about 0.05 s. After that, the displacement is almost zero in a steady state, i.e. the air gaps between stators and rotor are equal ($g_1 = g_2 = g_0$). The rotor now stands in the middle of two stators.

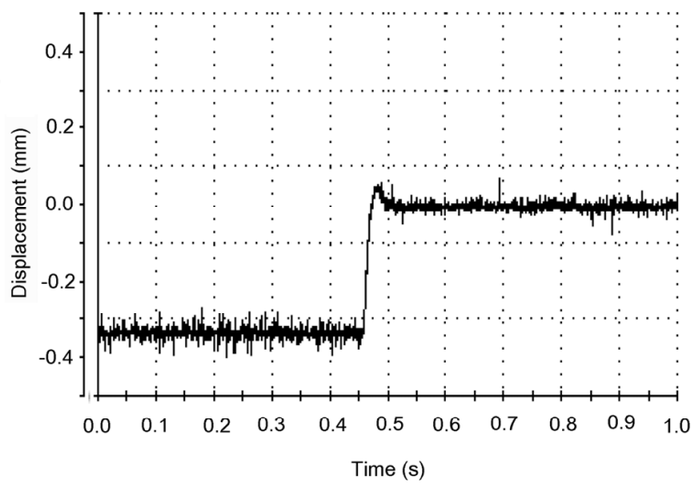

Fig. 17. Response of axial displacement at zero speed

Fig. 18 describes the change in the speed from zero to 6000 rpm and vice versa when the displacement is zero and the limited current is ±5A. The AGBM does not bear any load. With small starting time (about 0.7s) and stopping time (about 0.4s) the AGBM drive shows its good dynamic response.

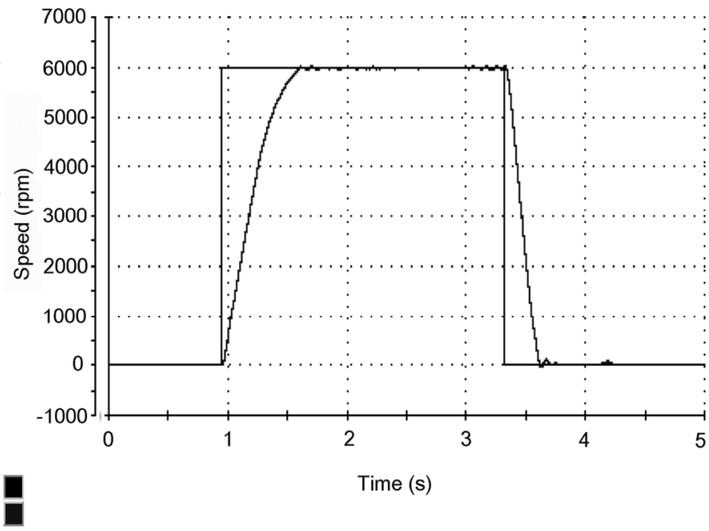

Fig. 18. Response of speed at zero displacement

Figs. 19 and 20 show response of the axial displacement and the speed when the AGBM starts to work. Initial displacement error is adjusted to 0.32mm, and the reference speed is 1500 rpm. When the AGBM operates, the displacement jumps immediately to zero. At the same time, the rotor speed increases and reaches 1500 rpm after 0.5s without influence of each other.
From above experimental results, it is obvious that the axial displacement and the speed are controlled independently with each other.
Fig. 21 illustrates the change of the direct axis current i_d, the quadrate axis current i_q, and the displacement when the motor speed changes from 1000 rpm to 1500 rpm and vice versa. The limited currents are set to ±3A. The AGBM drive works with rotational load. The rotational load is created by closing the terminals of a DC generator using a 1 Ω resistor. When the reference speed is changed from 1000 rpm to 1500 rpm, the q-axis current increases to the limited current. At the speed of 1500 rpm, the q-axis current is about 2.5A. Due to the influence of the q-axis current as shown in equation (18), there is little higher vibration in the displacement and the d-axis current at 1500 rpm. However, the displacement error is far smaller than the equilibrium air gap g_0, therefore the influence can be neglected.

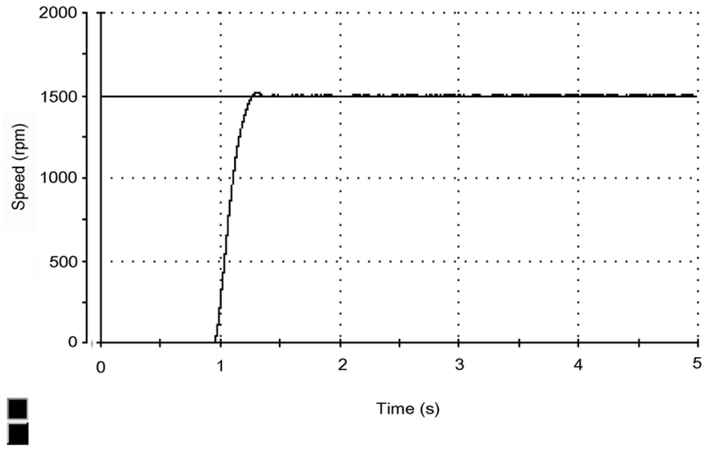

Fig. 19. Response of speed at start

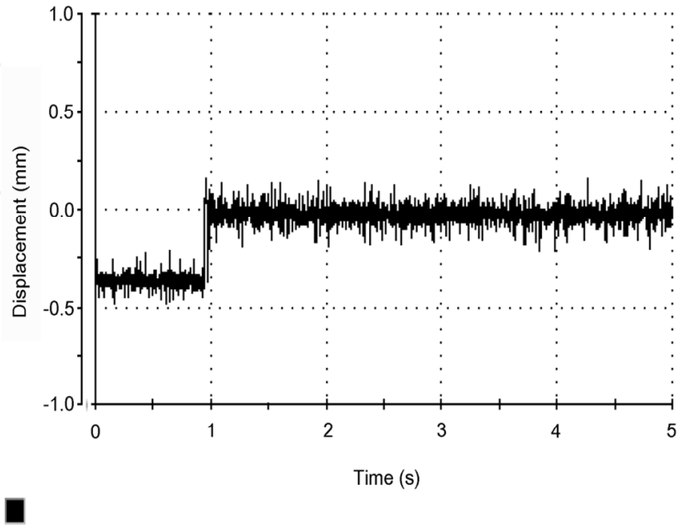

Fig. 20. Response of axial displacement at start

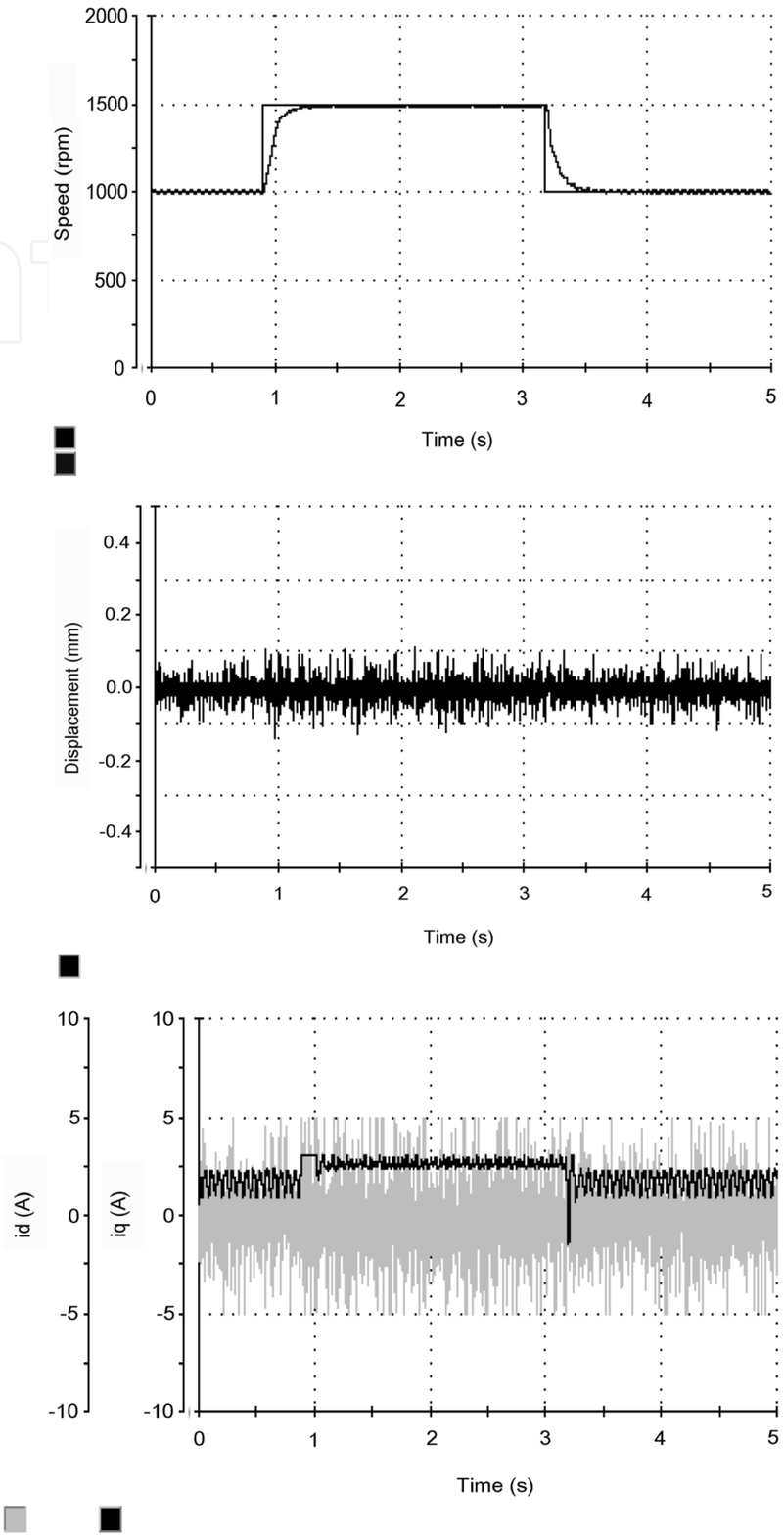

Fig. 21. Currents and displacement when rotor speed was changed

5. Conclusion

This chapter introduces and explains a vector control of the salient two-pole AGBM drives as required for high-performance motion control in many industrial applications.
Firstly, a general dynamic model of the AGBM used for vector control is developed, in which the saliency of the rotor is considered. The model development is based on the reference frame theory, in which all the motor electrical variables is transformed to a rotor field-oriented reference frame (d,q reference frame). As seen from the d,q reference frame rotating with synchronous speed, all stator and rotor variables become constant in steady state. Thus, dc values, very practical regarding DC motor control strategies, are obtained. Furthermore, by using this transformation, the mutual magnetic coupling between d- and q-axes is eliminated. The stator current in d-axis is only active in the affiliated windings of the d-axis, and the same applies for the q-axis.
Secondly, the vector control technique for the AGBM drives is presented in detail. In spite of many different control structures available, the cascaded structure, inner closed-loop current control and overlaid closed-loop speed and axial position control, is chosen. This choice guarantees that the AGBM drive is closed to the modern drives, which were developed for the conventional motors. Furthermore, the closed-loop vector control method for the axial position and the speed is developed in the way of eliminating the influence of the reluctance torque. The selection of suitable controller types and the calculation of the controller parameters, both depending on the electrical and mechanical behavior of the controlled objects, are explicitly evaluated.
Finally, the AGBM was fabricated with an inset PM type rotor, and the vector control with decoupled d- and q-axis current controllers was implemented based on dSpace DS1104 and Simukink/Matlab. The results confirm that the motor can perform both functions of motor and axial bearing without any additional windings. The reluctance torque and its influence are rejected entirely. Although, there is very little interference between the axial position control and speed control in high speed range and high rotational load, the proposed AGBM drive can be used for many kind of applications, which require small air gap, high speed and levitation force.

6. References

Aydin M.; Huang S. and Lipo T. A. (2006). Torque quality and comparison of internal and external rotor axial flux surface-magnet disc machines. IEEE Transactions on Industrial Electronics, Vol. 53, No. 3, June 2006, pp. 822-830.

Chiba A.; Fukao T.; Ichikawa O.; Oshima M., Takemoto M. and Dorrell D.G. (2005). *Magnetic Bearings and Bearingless Drives*, 1st edition, Elsevier, Burlington, 2005.

Dussaux M. (1990). The industrial application of the active magnetic bearing technology, *Proceedings of the 2nd International Symposium on Magnetic Bearings*, pp. 33-38, Tokyo, Japan, July 12–14, 1990.

Fitzgerald A. E.; C. Kingsley Jr. and S. D. Uman (1992). *Electric Machinery*, 5th edition, McGraw-Hill, New York,1992.

Gerd Terörde (2004). *Electrical Drives and Control Techniques*, first edition, ACCO, Leuven, 2004.

Grabner, H.; Amrhein, W.; Silber, S. and Gruber, W. (2010). Nonlinear Feedback Control of a Bearingless Brushless DC Motor. *IEEE/ASME Transactions on Mechatronics*, Vol. 15, No. 1, Feb. 2010, pp. 40 – 47.

Horz, M.; Herzog, H.-G. and Medler, N., (2006). System design and comparison of calculated and measured performance of a bearingless BLDC-drive with axial flux path for an implantable blood pump. *Proceedings of International Symposium on Power Electronics, Electrical Drives, Automation and Motion*, (SPEEDAM), pp.1024 – 1027, May 2006.

Kazmierkowski M. P. and Malesani L. (1998). Current control techniques for three-phase voltage-source PWM converters: a survey. IEEE Transactions on Industrial Electronics, Vol. 45, No. 5, Oct. 1998, pp. 691-703.

Marignetti F.; Delli Colli V. and Coia Y. (2008). Design of Axial Flux PM Synchronous Machines Through 3-D Coupled Electromagnetic Thermal and Fluid-Dynamical Finite-Element Analysis," *IEEE Transactions on Industrial Electronics*, Vol. 55, No. 10, pp. 3591-3601, Oct 2008.

Nguyen D. Q. and Ueno S. (2009). Axial position and speed vector control of the inset permanent magnet axial gap type self bearing motor. *Proceedings. of the International Conference on Advanced Intelligent Mechatronics* (AIM2009), pp. 130-135, Singapore, July 2009. (b)

Nguyen D. Q. and Ueno S. (2009). Sensorless speed control of a permanent magnet type axial gap self bearing motor. *Journal of System Design and Dynamics*, Vol. 3, No. 4, July 2009, pp. 494-505. (a)

Okada Y.; Dejima K. and Ohishi T. (1995). Analysis and comparison of PM synchronous motor and induction motor type magnetic bearing, *IEEE Transactions on Industry Applications*, vol. 32, Sept./Oct. 1995, pp. 1047-1053.

Okada, Y.; Yamashiro N.; Ohmori K.; Masuzawa T.; Yamane T.; Konishi Y. and Ueno S. (2005). Mixed flow artificial heart pump with axial self-bearing motor. *IEEE/ASME Transactions on Mechatronics*, Vol. 10, No. 6, Dec. 2005, pp. 658 – 665.

Oshima M.; Chiba A.; Fukao T. and Rahman M. A. (1996). Design and Analysis of Permanent Magnet-Type Bearingless Motors. *IEEE Transaction on Industrial Electronics*, Vol. 43, No. 2, pp. 292-299, Apr. 1996. (b)

Oshima M.; Miyazawa S.; Deido T.; Chiba A.; Nakamura F.; and Fukao T. (1996). Characteristics of a Permanent Magnet Type Bearingless Motor. *IEEE Transactions on Industry Applications*, Vol. 32, No. 2, pp. 363-370, Mar./Apr. 1996. (a)

Schneider, T. and Binder, A. (2007). Design and Evaluation of a 60000 rpm Permanent Magnet Bearingless High Speed Motor. *Proceedings on International Conference on Power Electronics and Drive Systems*, pp. 1 – 8, Bangkok, Thailand, Nov. 2007.

Ueno S. and Okada Y. (1999). Vector control of an induction type axial gap combined motor-bearing. *Proceedings of the IEEE International Conference on Advanced Intelligent Mechatronics*, Sept. 19-23, 1999, Atlanta, USA, pp. 794-799.

Ueno S. and Okada Y. (2000). Characteristics and control of a bidirectional axial gap combined motor-bearing. *IEEE Transactions on Mechatronics*, Vol. 5, No. 3, Sept. 2000, pp. 310-318.

Zhaohui Ren and Stephens L.S. (2005). Closed-loop performance of a six degree-of-freedom precision magnetic actuator, *IEEE/ASME Transactions on Mechatronics*, Vol. 10, No. 6, Dec. 2005 pp. 666 – 674.

IntechOpen

Magnetic Bearings, Theory and Applications

Edited by Bostjan Polajzer

ISBN 978-953-307-148-0

Hard cover, 132 pages

Publisher Sciyo

Published online 06, October, 2010

Published in print edition October, 2010

The term magnetic bearings refers to devices that provide stable suspension of a rotor. Because of the contact-less motion of the rotor, magnetic bearings offer many advantages for various applications. Commercial applications include compressors, centrifuges, high-speed turbines, energy-storage flywheels, high-precision machine tools, etc. Magnetic bearings are a typical mechatronic product. Thus, a great deal of knowledge is necessary for its design, construction and operation. This book is a collection of writings on magnetic bearings, presented in fragments and divided into six chapters. Hopefully, this book will provide not only an introduction but also a number of key aspects of magnetic bearings theory and applications. Last but not least, the presented content is free, which is of great importance, especially for young researcher and engineers in the field.

InTech Europe

University Campus STeP Ri
Slavka Krautzeka 83/A
51000 Rijeka, Croatia
Phone: +385 (51) 770 447
Fax: +385 (51) 686 166
www.intechopen.com

InTech China

Unit 405, Office Block, Hotel Equatorial Shanghai
No.65, Yan An Road (West), Shanghai, 200040, China
中国上海市延安西路65号上海国际贵都大饭店办公楼405单元
Phone: +86-21-62489820
Fax: +86-21-62489821

IntechOpen